DATA DESCRIPTOR

3D topographies and vibration signals of end-milling states including stable, forced vibration and chatter

Abstract

Vibration significantly impacts precision machining processes, adversely affecting surface quality, dimensional accuracy, and tool durability. Analyzing 3D topography of machined surface enables the identification and quantification of vibration information, essential for machining optimization. To support such investigations, a milling dataset was created in this study, comprising detailed 3D surface topography from end milling of 7075 aluminum alloy under diverse cutting conditions, including varying feed rates, spindle speeds, and machining states (stable cutting, forced vibration, and chatter). High-resolution surface data were acquired using white-light interferometry alongside synchronized acceleration signals collected during machining, which has seldom been reported in previous literature. These signals underwent frequency-domain analysis using Fast Fourier Transform (FFT) to determine peak frequencies, amplitudes, and their distributions, effectively characterizing vibration intensity and dynamic behavior. The dataset provides critical insights into relationships between machining parameters and process stability, establishing foundational knowledge for targeted improvements. The milling dataset thus facilitates research into machining stability, aiding in the development of precise control and optimization strategies.

Authors & Affiliations

Heng Wu[1], Pingfa Feng[1,2], Zhen Zhu[1], Chunmei Wu[1], Qiaochu Liu[2,3], Min Zhang[1], Feng Feng[1,*]

[1] Division of Intelligent Instrument and Equipment, Shenzhen International Graduate School, Tsinghua University, Shenzhen 518055, China

[2] Department of Mechanical Engineering, Tsinghua University, Beijing 100084, China

[3] AVIC Chengdu Aircraft Industrial (Group) Co., Ltd., Chengdu 610073, China

* Correspondence E-mail: feng.feng@sz.tsinghua.edu.cn; ORCID: 0000-0002-3960-7761.

Background & Summary

Vibration in machining is commonly classified into free, forced, and self-excited forms[1,2], each requiring distinct suppression strategies[3]. To identify the source and nature of vibration, a fundamental and widely adopted approach is time–frequency analysis[4-8]. In the time domain, global trends and abrupt changes are examined[4,8], whereas in the frequency domain Fast Fourier Transform (FFT)[5,9-12] is applied to extract spectral features—such as dominant frequencies and bandwidths—that reveal periodic vibration patterns[6]. Classical techniques, however, have limited capability when handling non-stationary signals and may fail to capture more complex characteristics[1]. To extract such features, several advanced algorithms have been introduced. McIntyre *et al.* proposed Short-Time Fourier Transform (STFT) segments the signal to reveal frequency variations over time[13]; Empirical Mode Decomposition (EMD) combined with the Hilbert–Huang Transform (HHT)[14,15] which was proposed by Huang *et al.* decomposes strongly nonlinear signals into intrinsic mode functions[16], from which instantaneous frequency and energy can be derived. In addition, modern machine-learning methods—such as long short-term memory (LSTM) networks[17-20] and attention-based models[21-25]—have been widely employed, because they can detect correlations within long sequences and therefore better highlight factors that induce vibration. Vashisht *et al.* improved the cutting-dynamics equations to simulate CNC ball-screw drive-current sequences and used them to train an LSTM network, thereby enabling on-line chatter detection in milling without additional sensors; an experimental accuracy of 98 % was reported[26].

Most existing studies rely heavily on time-series signals such as acceleration or acoustics and often require stability-lobe diagrams to assess system stability[9,27-29]. This practice is disadvantageous for chatter—an especially harmful self-excited vibration—because stability lobes merely indicate whether chatter occurs and cannot quantify its severity[30]. Consequently, parameter selection in actual machining remains ambiguous, and empirical or conservative strategies continue to dominate.

Given that the ultimate objective is the workpiece surface, intermediate signals such as vibration, force, and sound are merely investigative tools rather than final targets. Guided by an end-to-end philosophy, recent research has focused on direct surface monitoring[31-33]; for example, Wu *et al.* developed a ToolWearNet convolutional-neural-network[34] model that was first pre-trained with a convolutional auto-encoder and subsequently fine-tuned by back-propagation with stochastic gradient descent; in on-line machine-tool experiments, the method achieved 96.20 % accuracy in classifying tool-wear types and limited the mean absolute percentage error of wear-value estimation to 4.76 %, thereby demonstrating high efficiency and practical applicability. Xiao *et al.* introduced an end-to-end CNN-BiTCN-Attention model[35] that integrates a convolutional neural network, a bidirectional temporal convolutional network, and an attention mechanism. On the public ACF dataset, the proposed approach achieved a mean absolute percentage error of 0.79 % and a coefficient of determination of 99.81 % for surface-roughness prediction, outperforming existing methods by a considerable margin. With this motivation, the 7075milling dataset was collected, providing surface morphology produced under diverse milling parameters for 7075 aluminum alloy. Three-dimensional surface maps were acquired with a surface profilometer and compiled into high-resolution point-cloud data that reveal fine surface details. The dataset offers paired information on surface topography and synchronized spindle-acceleration signals for various machining states, comprising 1 160 sets of 3D topography and corresponding acceleration data. Dominant frequencies in the acceleration signals were extracted via FFT.

In previously released datasets, topography is often obtained by laser scanning[36], whose resolution is lower than that of white-light interferometry and may obscure surface details, while many studies disclose only acceleration data without surface information. 7075milling, by contrast, delivers finer 3D surface detail. In the work of Zhou *et al.*[37], these surface maps were used to train a CNN capable of identifying and quantifying chatter features; the resulting metrics enabled selection of more efficient cutting parameters without compromising quality. Moreover, the classification accuracy of this method is 100% based on experimental data, which is higher than that of G_a(97.7%), APSD(79.5%), and OV (97.7%) methods. Zhu *et al.*[38] employed the dataset to separate self-excited and forced vibration components—phenomena that differ in origin, energy, and mitigation measures. Energy analysis quantified each vibration mode's influence on the surface, and several spatial-frequency components combined with acceleration signals were used to approximate the overall surface profile, although detailed reconstruction remained elusive—again underscoring the importance of retaining raw surface data.

Method

Introduction. The Methods section is structured as follows: first, the experimental platform used for data acquisition is introduced; then, the machining procedures and data collection methods are described; finally, the preprocessing steps applied to ensure temporal alignment and to extract valid data segments are presented.

The Experimental Setup. As shown in Figure 1, experiments were conducted on a EUMA DU810 vertical machining center using 8 mm diameter two-flute carbide end mills with a 40 mm overhang. Slot milling was performed on 7075 aluminum alloy workpieces (150 mm × 150 mm) under varying process conditions: spindle speed (3000–10000 rpm), feed rate (300–2000 mm/min), axial depth of cut ap = 1 mm, and radial depth of cut ae = 8 mm. Fifty-eight unique parameter combinations were tested.

Data Acquisition.

- **Surface Data Acquisition.** 3D surface data were captured using an RTEC white-light interferometer … 946 mm … 1.216

- **Acceleration Data Acquisition.** Acceleration data were recorded at 25.6 kHz using a PCB triaxial piezoelectric accelerometer connected to an LMS SCADAS Mobile 05 DAQ system. Signal preprocessing involved noise removal, temporal alignment, and segmentation based on effective cutting intervals. Surface data were also denoised by filtering extreme Z outliers caused by surface contaminants or measurement artifacts.

- **Coordinate System Setup.** Since a fixed coordinate system is required during machining, measurement, and signal acquisition, this study defines a global coordinate system as follows: the y-axis points opposite to the feed direction during machining, the x-axis lies within the machining plane and is perpendicular to the y-axis; and the z-axis is perpendicular to the machining plane.

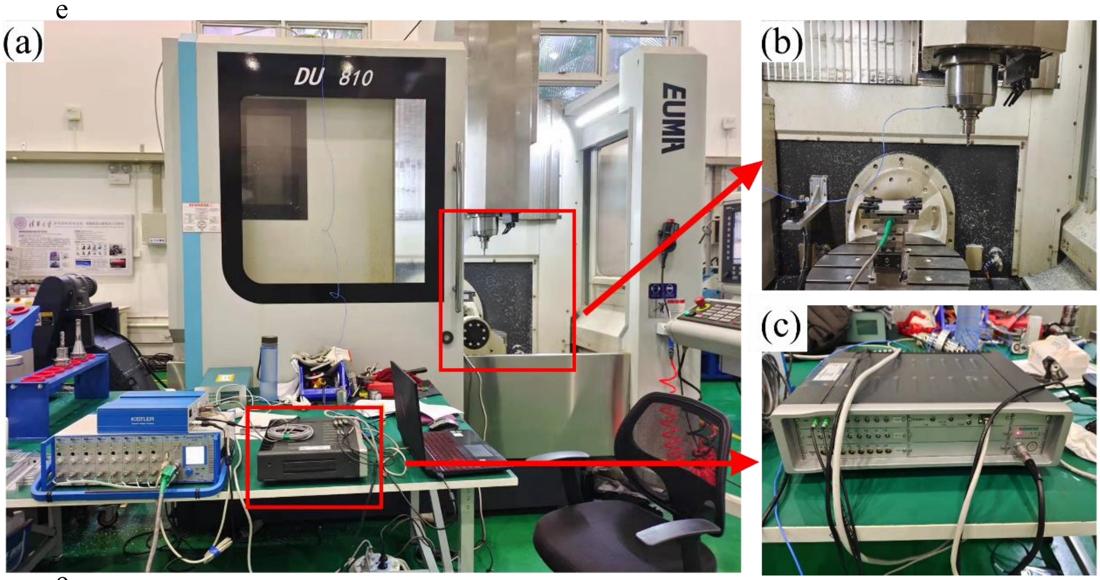

Figure 1. Experimental platform: (a) EUMA DU810 vertical machining center; (b) worktable; (c) LMS SCADAS Mobile 05.

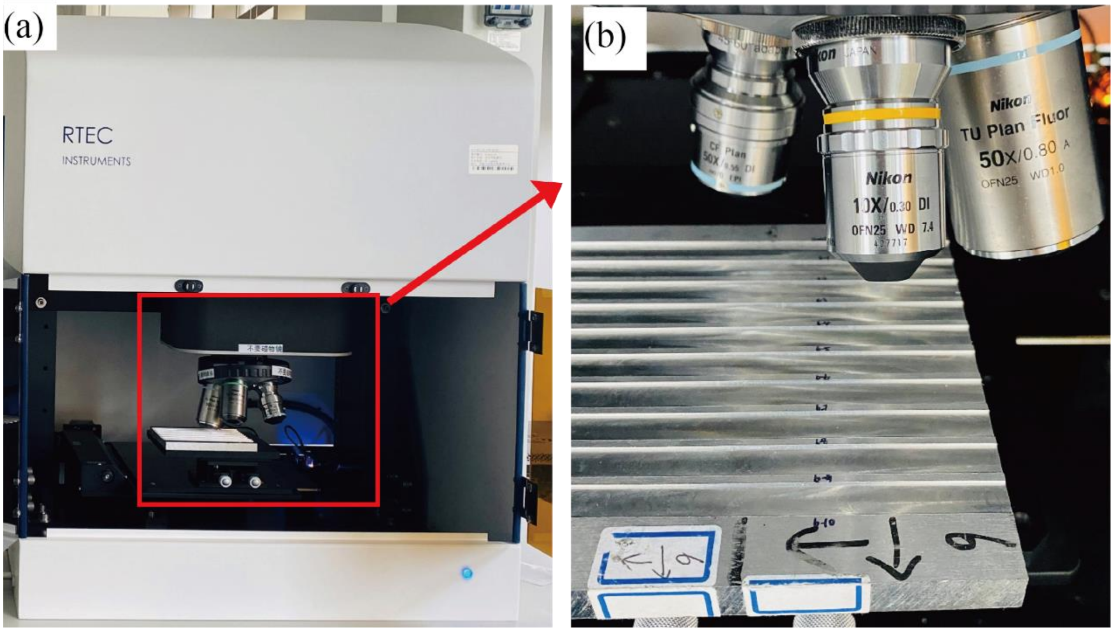

Figure 2. Surface topography measurement platform: (a) RTEC 3D surface profilometer; (b) worktable.

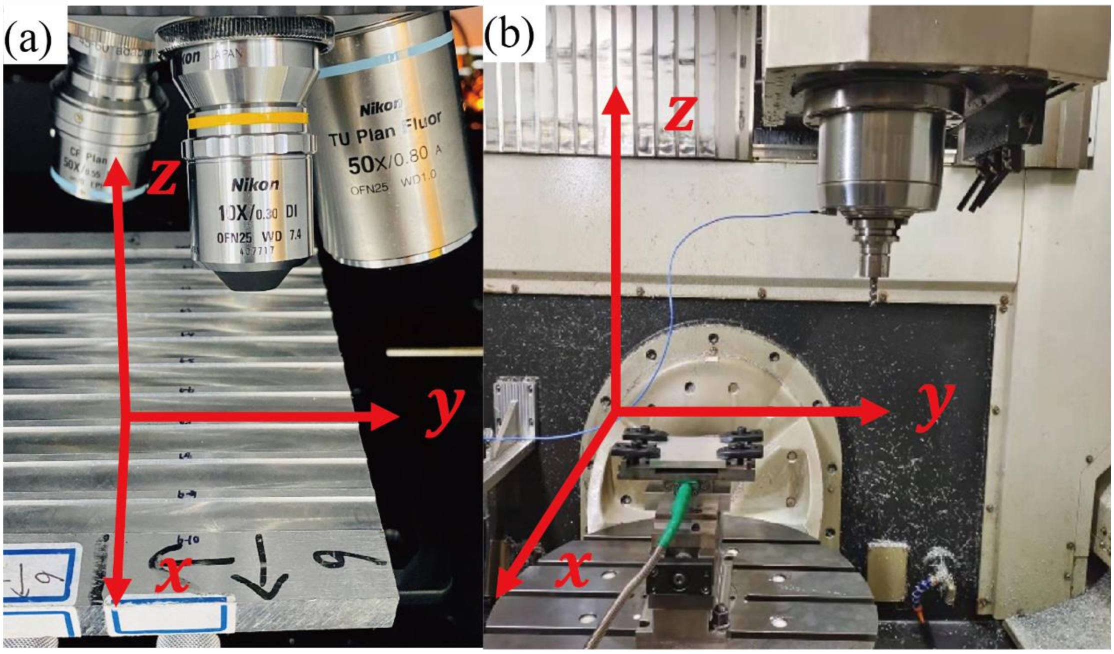

Figure 3. Definition of the global coordinate system: (a) Representation of the global coordinate system during surface data acquisition; (b) Representation of the global coordinate system during machining and acceleration signal acquisition.

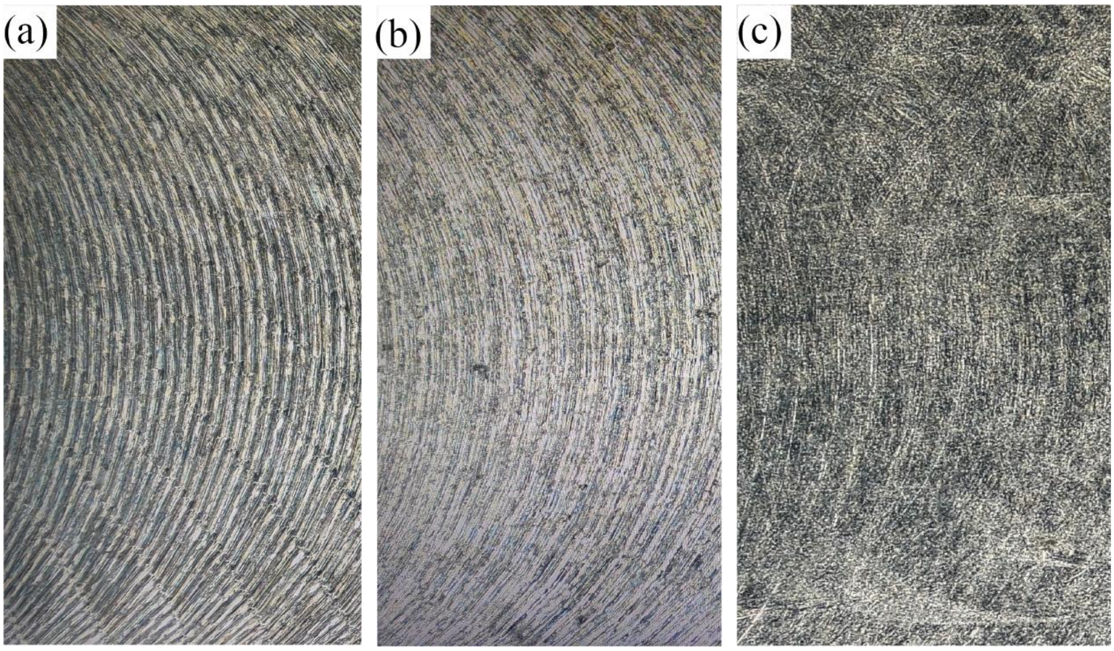

Figure 4. Microscopic view of the machined surface: (a) chatter surface; (b) forced vibration surface; (c) stable surface.

Spindle speed n range (rpm)	Spindle speed step (rpm)	Feed rate f range (mm/min)	Feed rate step (mm/min)
3000-6000	1000	300-1300	100
7000, 10000	/	300-2000	100
11000, 12000	/	300, 1300, 1800	/

Table 1. Machining parameters used in the experiments

The raw data collected during the experiments, including surface topography and acceleration signals, required cropping and alignment before being used for subsequent research, as it would otherwise be impossible to determine temporal correspondence between datasets. To achieve alignment, the acceleration signals were first segmented according to the actual cutting process, retaining only the valid portions. During surface data acquisition, 20 surface profiles were obtained from each slot-milled groove, and the distance from each acquisition point to the groove start was recorded. Given the known feed rate, the machining time corresponding to each surface profile could be calculated, enabling synchronization with the acceleration signal at the same time point. The surface data were also denoised by removing extreme outliers in Z-values, which typically resulted from residual contaminants or accidental scratches.

The resulting 3D surface topography is shown in the corresponding figure. Likewise, the acceleration signals acquired during each experiment are displayed. In Figure (a), the raw acceleration data are shown. The actual machining duration is enclosed between two bold dashed lines, while the regions outside correspond to idle noise recorded during non-cutting periods. From the valid acceleration signal, 20 equally spaced segments were extracted, each aligned with one of the 20 surface profiles collected per slot. Thus, each marked point on the acceleration signal corresponds to a specific surface profile acquired at that time.

Signal preprocessing involved noise removal, temporal alignment, and segmentation based on effective cutting intervals. Surface data were also denoised by filtering extreme Z outliers caused by surface contaminants or measurement artifacts.

In the 7075milling dataset, the maximum spindle speed used in the experiments is 12000 rpm, which corresponds to a tooth-passing frequency of 400 Hz for the two-flute milling tool. Specifically, the frequency range most influential to surface characteristics in these experiments lies within a few hundred hertz. Consequently, the primary focus is on frequencies below 1000 Hz.

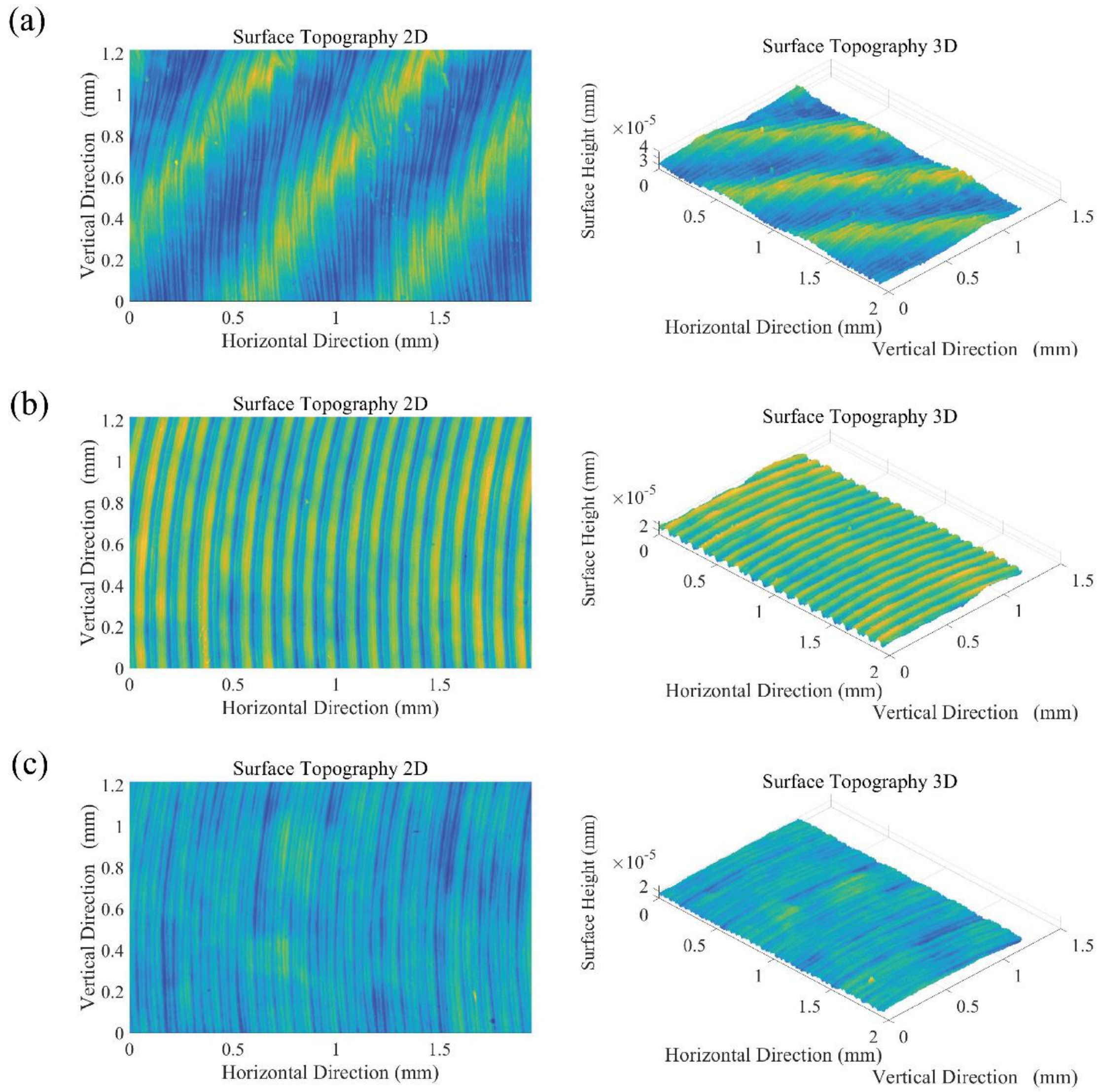

Figure 5. 3D topography of the machined surface: (a) chatter surface; (b) forced vibration surface; (c)

stable surface.

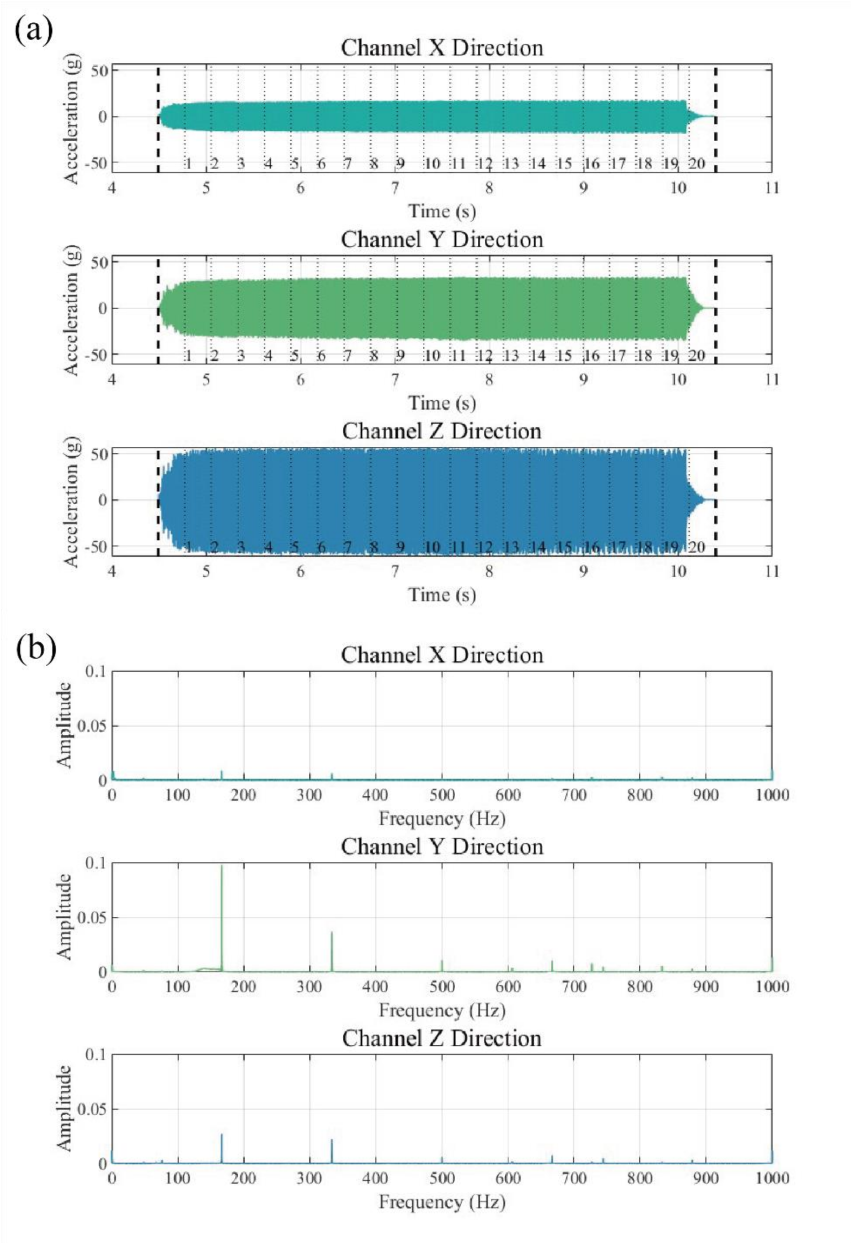

Figure 6. Acceleration signals during the machining process: (a) raw acceleration data; (b) FFT-processed acceleration data.

Data Record

The structure of the 7075milling dataset is depicted in Figure 6. The root directory contains all data files together with visualization scripts for surface topography and vibration-acceleration signals. These scripts serve as basic templates, enabling users to explore and interpret the dataset in detail. Each filename includes an index in the format “3-1,” “5-7,” and so forth: the numeral before the dash (3 – 7) denotes an individual workpiece, whereas the numeral after the dash (1 – 10) identifies a specific slot-milled surface on that workpiece. In addition, the root directory houses EXP20211020Data_path.mat, a file that consolidates all database information to facilitate convenient data access.

AccSeg. The AccSeg folder contains the trimmed vibration-acceleration signal segments. Each segment corresponds to one 3D surface-topography record. This correspondence is established via the index numbers in the filenames: files sharing the same index and sequence number constitute a complete pair of surface and acceleration data. The signals were sampled at 25.6 kHz (time increment ≈ 3.90625×10^{-5} s), yielding 368 907 samples that span approximately 1.72691×10^{-5} s to 14.4104 s. Acceleration is reported in units of g; both hardware and user voltage ranges are ± 10 V with a zero bias of 0 g, and the data are stored as real numbers. Three channels represent acceleration components at the same measurement point along +X (C1), –Y (C2), and –Z (C3) directions, with sensitivities of 10.59 $\mathrm{mV \cdot g^{-1}}$, 10.42 $\mathrm{mV \cdot g^{-1}}$, and 10.13 $\mathrm{mV \cdot g^{-1}}$, respectively.

FFTSeg. The FFTSeg folder contains the FFT results of the trimmed vibration-acceleration signals. Each file comprises three columns—frequency, amplitude, and phase. The amplitude represents the energy intensity of the corresponding frequency component in the original signal (conversion to a power spectrum requires squaring or other normalization), whereas the phase indicates the time-zero phase offset at that frequency component.

EXP20211020Data_path.mat. The file contains a table-type variable named EXP20211020Data_path, which stores all experimental parameters as well as the paths to the raw data files. Embedding the raw data themselves would slow down the program, so only path indices are provided; the accompanying scripts can then use these paths to access every raw data file with ease.

three_dimension_topography. three_dimension_topography contains the 3D surface topography data of the machined workpieces. Each row in a matrix corresponds to a horizontal scan across the measurement grid (960 sample points), and each column corresponds to a vertical scan (600 lines). As a result, each matrix is a 600×960 array storing only the Z-values representing surface height.

update_path_prefixes.m. change_file_path.m is a MATLAB script used to update all file path references in the dataset so that they point to the user's current working directory.

EXP20211020Data_path.mat. EXP20211020Data_path.mat stores all data related to the 7075milling dataset, including experimental parameters and corresponding results. This file contains a variable named EXP20211020Data_path, which is of table type. Each column in this table stores a specific type of data, as detailed in the accompanying documentation. One of the columns, real_surf, contains nested table-type variables, where each subtable includes multiple columns representing detailed attributes associated with the surface topography and corresponding acceleration segments.

visualize_3D_topography.m. This program is used to visualize the surface topography. The resulting output includes both 2D and 3D images.

visualize_acc_fft_seg.m. This program is used to visualize the acceleration segments and their corresponding FFT segments.

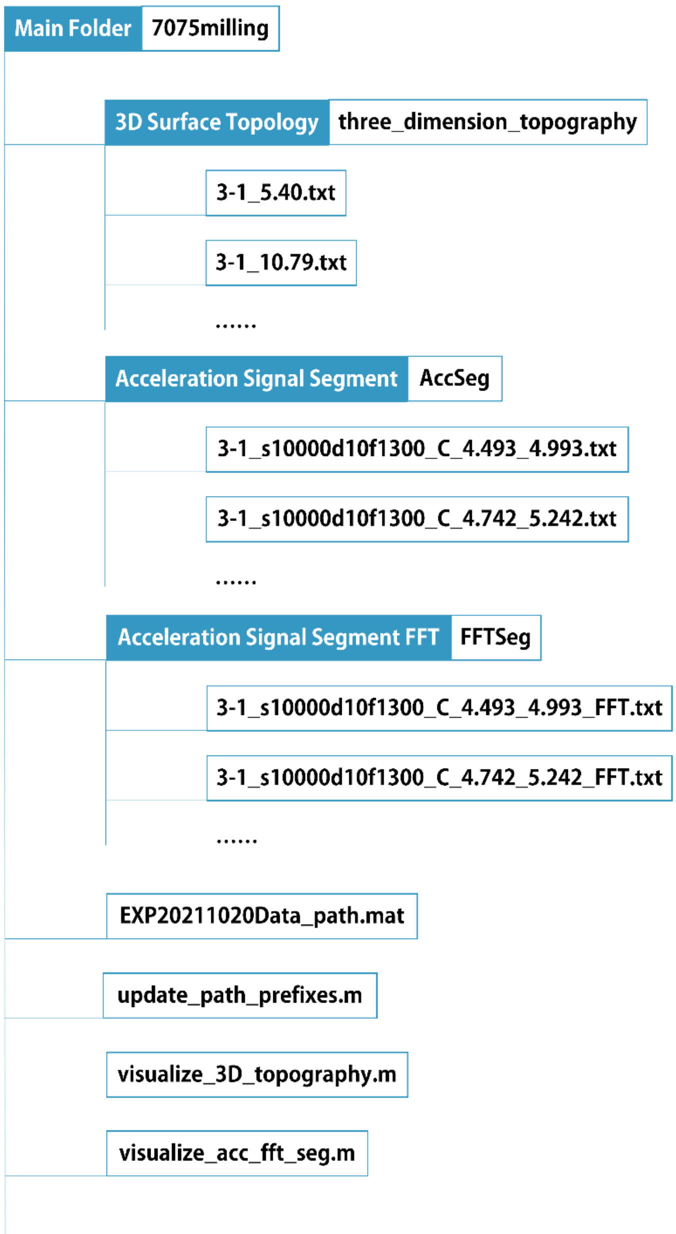

Figure 7. Structure of the dataset.

Column Name	**Description**
s_r_min	Spindle speed (rpm)
d_0_1m	Axial depth of cut ap (in 0.1 mm units; e.g., 10 = 1 mm)

m	
f_mm_min	Feed rate (mm/min)
f_t_mm_tooth	Feed per tooth / chip load (mm/tooth)
acc_start	Actual start time of milling (seconds)
acc_end	Actual end time of milling (seconds)
real_surf	W h i
status	Chatter status label ('C': chatter, 'U': unclear, 'F': forced vibration, 'S': stable)

Table 2. Description of each column in EXP20211020Data_path

Column Name	Description
path_to_surf_data	File path to the original white-light matrix data
position	Surface profile location identifier
start	Milling start time (s)
end	Milling end time (s)
path_to_acc_seg	File path to corresponding segmented acceleration data
path_to_fft_seg	File path to corresponding FFT of acceleration data
ra	Measured surface roughness Ra (m)

Table 3. Description of each column in real_surf

Technical Validation

To demonstrate the feasibility and novelty of interpreting machining processes directly from surface data using the 7075milling dataset, data-quality verification is performed from several perspectives. First, the surface topography is transformed into the frequency domain through two-dimensional Fast Fourier Transform (2D-FFT) and power spectral density (PSD) analysis; the dominant spatial frequency is then extracted to determine whether it matches the machining parameters[39,40].

The rationale for validating parameter consistency via the dominant spatial frequency is as follows. A surface map from the dataset is selected, and the global mean of the raw signal is shifted to zero to eliminate offsets introduced by instrument drift or large-scale form error. The mean value is calculated using Eq. (1),

$$\mu = \frac{1}{N_x N_y} \sum_{x=1}^{N_x} \sum_{y=1}^{N_y} Z(x, y) \tag{1}$$

then differencing is applied to eliminate any residual bias as Eq. (2).

$$Z_{\text{bias removed}}(x, y) = Z(x, y) - \mu \tag{2}$$

To ensure that peak detection and energy comparison across different samples are performed on a consistent scale and remain unaffected by absolute amplitude, the bias-corrected signal is further normalized by division by its standard deviation.

$$\sigma = \sqrt{\frac{1}{N_x N_y} \sum_{x,y} \left(Z_{\text{bias removed}}(x, y)\right)^2}, Z_{\text{norm}}(x, y) = \frac{Z_{\text{bias removed}}(x, y)}{\sigma} \tag{3}$$

Windowing was subsequently applied by multiplying the bias-corrected image with Hamming (Hann) windows in the horizontal and vertical directions, thereby generating a two-dimensional window function $w(x, y)$ that provides smooth transitions at the image boundaries and maximally suppresses spectral-leakage effects. The windowed image, $Z_w(x, y) = Z(x, y) \cdot w(x, y)$, was subjected to a two-dimensional Fast Fourier Transform (2D-FFT); a Fourier-shift operation was then performed to relocate the DC component to the centre of the spectrum, yielding a symmetrically distributed frequency map. The magnitude of this complex spectrum was squared to obtain the power-spectral-density matrix $\mathrm{PSD}(u, v)$, which quantitatively describes the energy distribution of each spatial-frequency component. Regional-maximum detection was subsequently conducted on the PSD image to identify local maxima; peaks at the global mean level were discarded, and a subset of candidate peaks representing significant periodic surface structures was retained.

For each detected peak, the offset between its pixel coordinates (u_i, v_i) and the spectrum centre (u_0, v_0) is normalised and converted into the spatial frequency (cycles · pixel^{-1}) as $\sqrt{\left((u_i - u_0)/N_x\right)^2 + \left((v_i - v_0)/N_y\right)^2}$. Using the known pixel-to-physical scale (960 px corresponding to 1.92 mm), the spatial frequency in cycles · mm^{-1} and its reciprocal wavelength can be derived. Given the feed rate $f_{\mathrm{mm/min}}$, the spatial wavelength divided by the feed speed is converted into the temporal frequency (Hz). This procedure yields a complete spatio-temporal spectral characterisation of the periodic surface features produced during machining. By comparing these calculated features with those expected from the machining parameters, surface consistency can be quantitatively evaluated.

Figure 7 presents the 2D-FFT output and the associated power-spectral-density (PSD) map; the extracted wavelengths are annotated in panel (a). To verify the consistency between the surface-profile data and the machining process, the analytically calculated tooth-passing frequency was compared with the tooth-passing frequency extracted from the PSD of the 7075milling dataset. The results indicate that 80 % of the samples exhibit relative errors below $25.52\ \%$. As illustrated in Figure 8, the portion to the left of the black dashed line represents the share of groups whose errors fall within this range, confirming good agreement between the 3D surface measurements and the experimental parameters. The first five harmonic orders derived from the surface morphology are shown in Figure 9.

After applying a Fast Fourier Transform (FFT) to the acceleration signals, the frequency spectrum and corresponding amplitudes were obtained, and the five leading frequency components below 1 kHz were extracted. To validate the consistency between surface topography and acceleration data, these five frequencies were compared with the chip-passing frequency derived from the surface measurements. Within a $\pm 10\ \%$ error margin, an accuracy of $81.03\ \%$ was achieved, meaning that 47 of the 58 groups were mutually consistent; the Pearson correlation coefficient reached $r = 0.93$. Figure 10 illustrates this comparison: the bars represent tooth-passing frequencies extracted from the surface topography, whereas the orange line denotes those obtained from the acceleration signals, clearly demonstrating strong agreement between the two datasets.

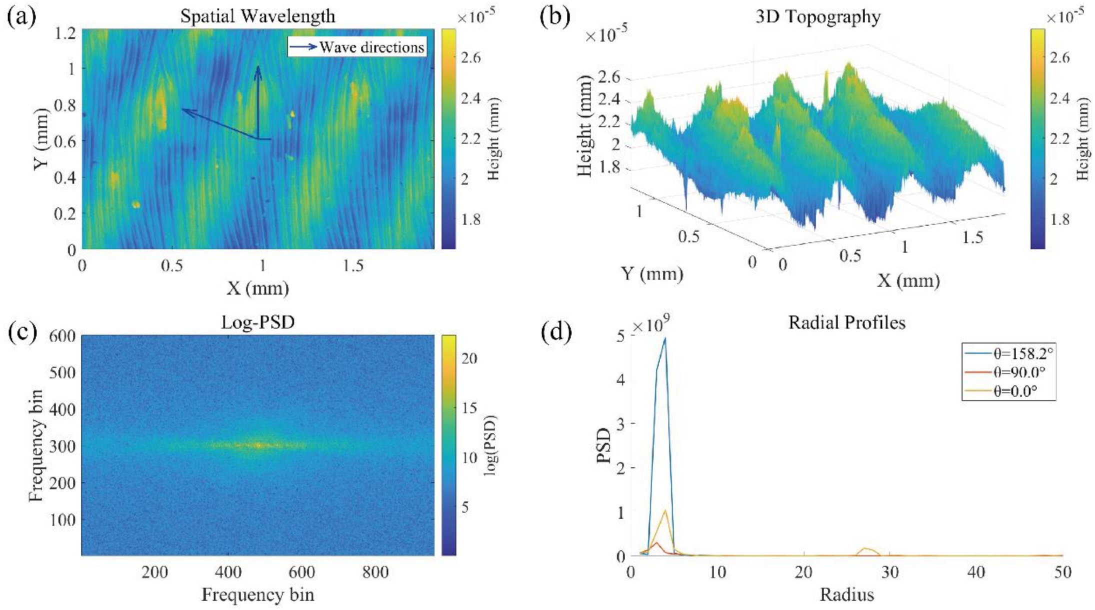

Figure 8. Periodic surface features extracted via 2D-FFT. (a) Raw surface data with the extracted wavelength annotated; (b) 3D surface topography; (c) Power spectrum of the original surface; (d) Profile of power spectral density curve as a function of frequency radius in each direction.

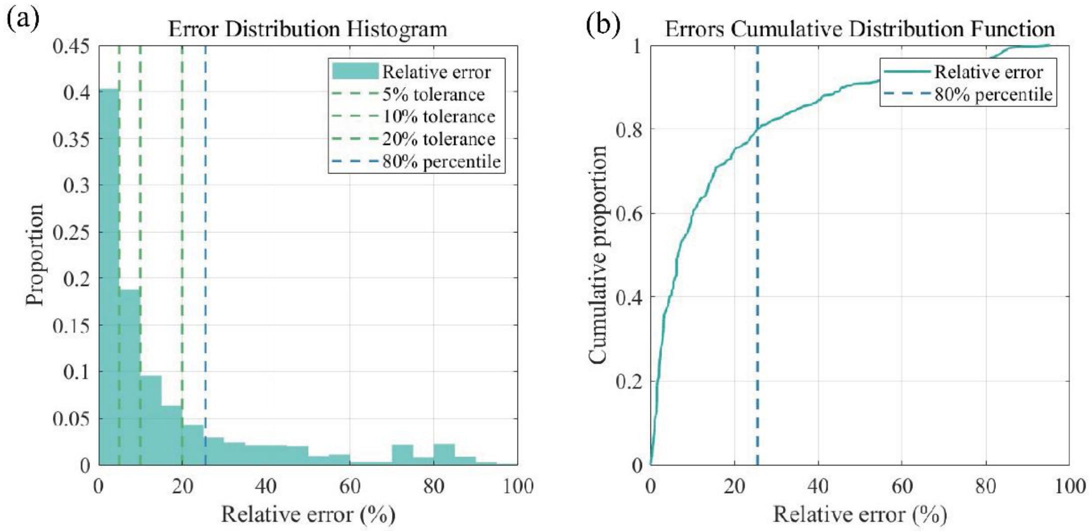

Figure 9 Relative error between the tooth-passing frequency extracted from the surface data and the theoretical tooth-passing frequency calculated from the machining parameters. (a) Histogram; (b) Cumulative Distribution.

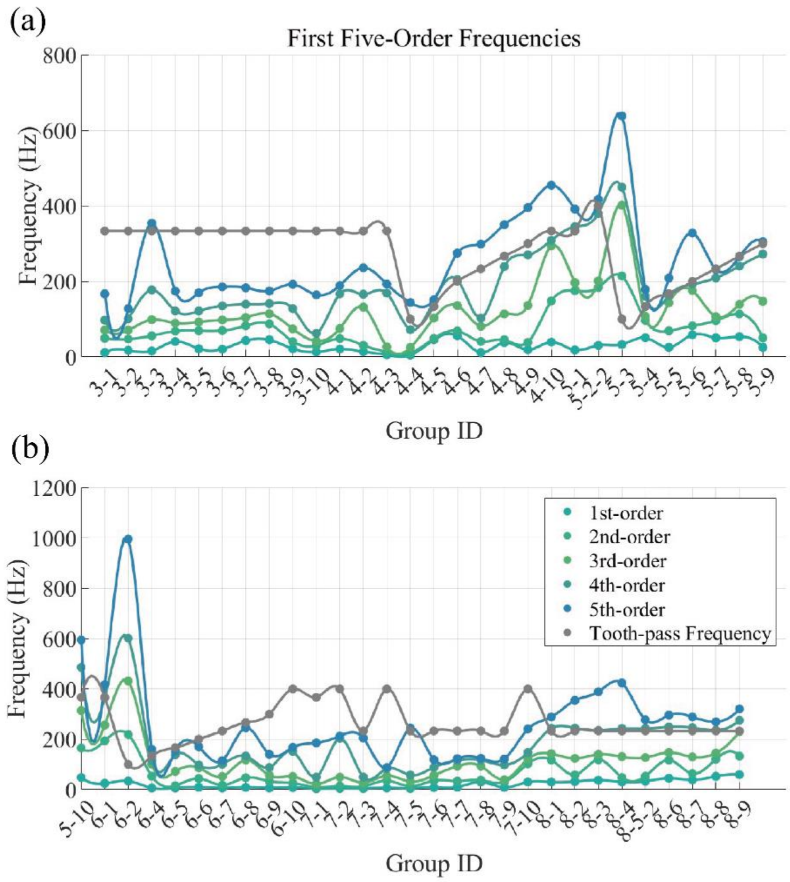

Figure 10. The top 5 dominant spatial frequencies extracted from each milled slot surface.

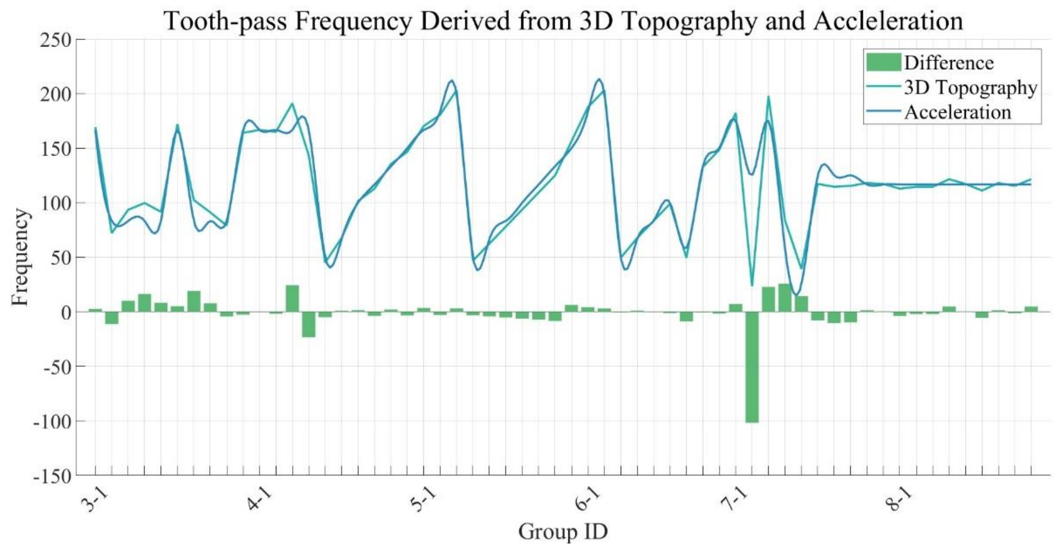

Figure 11. Correlation between the tooth-passing frequency extracted from the acceleration signals and that obtained from the surface data.

To validate the suitability of 7075milling for studying chatter—a vibration phenomenon of considerable interest in machining—and its manifestation in surface topography, an energy-based metric was developed. This metric incorporates the total vibration energy and can be decomposed into forced-vibration energy and self-excited-vibration energy[38,41]. It is extracted from the acceleration signals and compared with surface-roughness information derived from the topography, thereby assessing the dataset's effectiveness for chatter research.

The procedure is as follows. A one-dimensional convolutional neural network (1D-CNN) is employed to predict three parameters from the acceleration signal—amplitude A, spatial frequency ξ, and phase offset φ—that characterise the forced and self-excited vibration energies. With these parameters, the machined surface profile can be reconstructed, and the out-of-plane (Z-direction) height $z(x, y)$ at each surface coordinate can be calculated by Eqs. (4)–(6).

$$z_i = A_i \cdot \sin\big(2\pi \cdot \xi_i \cdot (\cos(\varphi_i) \cdot (x - \Delta) + \sin(\varphi_i) \cdot y)\big) \tag{4}$$

$$\Delta = r - \sqrt{r^2 - y^2} \tag{5}$$

$$z = \sum_{i=1}^{3} z_i \tag{6}$$

The out-of-plane height values, z, can be directly converted into the energy associated with forced and self-excited vibrations. In a machining system, the cutting tool is commonly modelled as an axial spring–mass system, whose elastic potential energy is expressed as $E = \frac{1}{2}Kx^2$ where K is the overall stiffness and x is the tool-tip displacement. Because the displacement at the tool tip is faithfully recorded in the milled surface profile, the reconstructed height z may be substituted for x to compute E. The overall stiffness is the sum of the tension-induced stiffness (K_{T}) and the bending stiffness (K_{B}) of the cutter, as given in Eqs. (7, 8). In these expressions, E_{m}denotes the Young's modulus of the tool material, while D and L represent the tool diameter and overhang length, respectively.

To remove the influence of differing surface dimensions and resolutions, the vibration energy is normalised by $1\ /\ N$, where $N\ (=\ n\ \times\ m)$ is the total number of grid points in the surface map. All calculations employ SI units: length in metres (m), spatial frequency in cycles per metre (cycles m^{-1}), Young's modulus in pascals (Pa), and energy in joules (J).

$$E = \frac{1}{N} \times \frac{1}{2} K \sum_{i=1}^{n} \sum_{j=1}^{m} z_{ij}^2 \tag{7}$$

$$K_{\mathrm{T}} = E_{\mathrm{m}} \times \frac{\pi D^2}{4L} \tag{8}$$

$$K_{\mathrm{B}} = \frac{3E_{\mathrm{m}} \cdot I}{L^3};\ \ I = \frac{\pi D^4}{64} \tag{9}$$

The one-dimensional CNN architecture used for prediction is illustrated in Figure 11. After energy separation, the results were compared with roughness values obtained from the measured surface topography; as shown in Figure 12, strong agreement is observed between the acceleration-based and surface-based estimates for both total energy and forced-vibration energy.

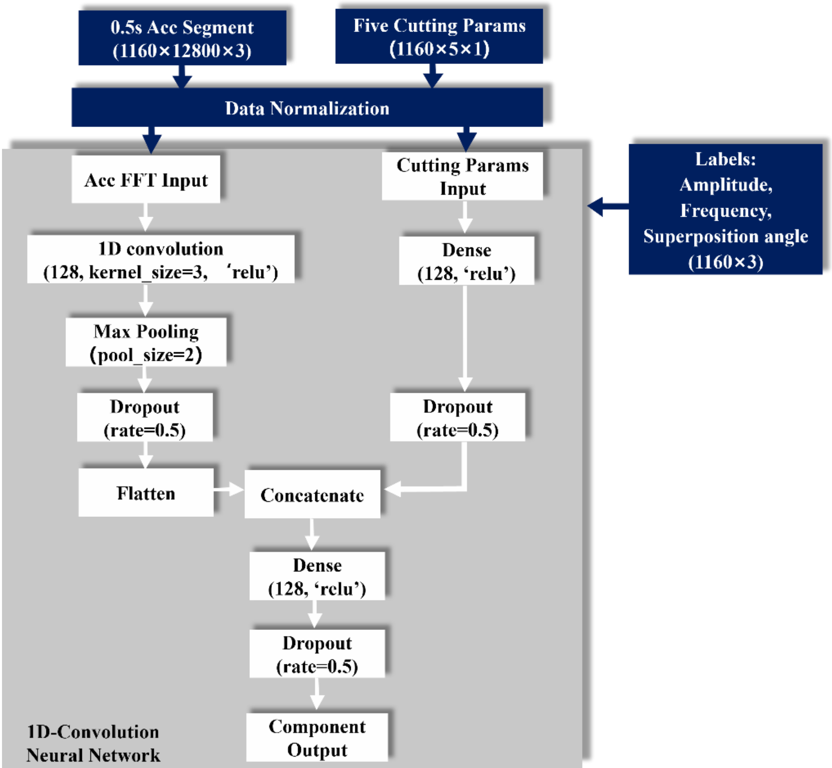

Figure 12. The structure of 1D-CNN

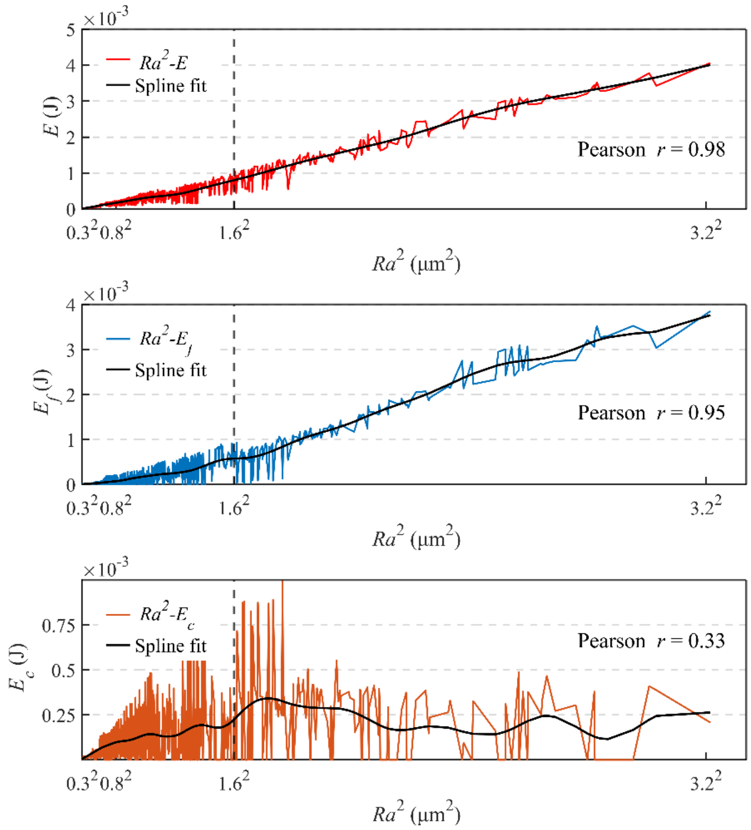

Figure 13. Correlation between vibration energy E, E_f, E_c and surface roughness squared Ra^2

Usage Notes

The 7075milling dataset is valuable for studying the stability of milling processes. It is particularly well-suited for applying machine learning methods to model the relationship between machining parameters and process stability. Given the complexity of how machining conditions affect final outcomes, such modeling enables the acquisition of insights into process optimization at low technical cost. In addition, the 7075milling dataset can be used for purely theoretical research. However, users should note that the surface morphology is also affected by the material properties of both the workpiece and the tool—an aspect that is not extensively addressed in this dataset. While the chatter-induced surface patterns observed in this dataset are generally consistent with Grossi's principle, subtle differences may arise depending on the specific machining system. Users are encouraged to consider such factors before application. The 7075milling database offers a rich source of data for the fields of machining, chatter, and surface topography. It is freely available to users under the applicable license, and any questions may be directed to the corresponding author to maximize the utility of this dataset.

Acknowledgements

This work was supported by National Natural Science Foundation of China under Grant No. 52275441 and Shenzhen Science and Technology Program under Grant No. KJZD20230923114606013.

Authorship contribution

Heng Wu: Writing – original draft, Investigation, Data curation. Pingfa Feng: Writing – review & editing, Investigation, Supervision. Zhen Zhu: Writing – review & editing, Investigation. Chunmei Wu: Writing – review & editing, Investigation. Qiaochu Liu: Conceptualization, Writing – review & editing, Investigation. Min Zhang: Writing – review & editing, Investigation. Feng Feng: Conceptualization, Writing – review & editing, Investigation.

Competing interests

The authors declare no competing interests.

Code Availability

All available code for this dataset is included in the root directory. All signal processing and visualization were performed in MATLAB (R2023a, The MathWorks Inc., USA).

Reference

1 Ding, H., Ding, Y. & Zhu, L. M. On time-domain methods for milling stability analysis. *Chinese Science Bulletin* **57**, 4336-4345 (2012). https://doi.org/10.1007/s11434-012-5499-y

2 Yan, X. L., Melkote, S., Mishra, A. K. & Rajagopalan, S. A digital apprentice for chatter detection in machining via human-machine interaction. *Journal of Intelligent Manufacturing* **34**, 3039-3052 (2023). https://doi.org/10.1007/s10845-022-01992-3

3 Chen, G. X., Li, Y. G., Liu, X. & Yang, B. Physics-informed Bayesian inference for milling stability analysis*. *International Journal of Machine Tools & Manufacture* **167** (2021). https://doi.org/10.1016/j.ijmachtools.2021.103767

4 Peng, C., Wang, L., Li, Z. Q. & Yang, Y. Q. Time-domain simulation and experimental verification of dynamic cutting forces and chatter stability for circular corner milling. *Proceedings of the*

Institution of Mechanical Engineers Part B-Journal of Engineering Manufacture **229**, 932-939 (2015). https://doi.org/10.1177/0954405414535585

5 Wang, C. X., Zhang, X. W. & Chen, X. F. Real time FFT identification based time-varying chatter frequency mitigation in thin-wall workpiece milling. *International Journal of Advanced Manufacturing Technology* **119**, 7403-7413 (2022). https://doi.org/10.1007/s00170-022-08755-7

6 Gupta, P. & Singh, B. in *1st International Conference on Energy, Materials Sciences and Mechanical Engineering (EMSME).* 640-645 (2021).

7 Ko, J. H. & Shaw, K. C. Chatter prediction based on frequency domain solution in CNC pocket milling. *International Journal of Precision Engineering and Manufacturing* **10**, 19-25 (2009). https://doi.org/10.1007/s12541-009-0067-3

8 Ding, Y., Zhu, L. M., Zhang, X. J. & Ding, H. Second-order full-discretization method for milling stability prediction. *International Journal of Machine Tools & Manufacture* **50**, 926-932 (2010). https://doi.org/10.1016/j.ijmachtools.2010.05.005

9 Suzuki, N., Kurata, Y., Kato, T., Hino, R. & Shamoto, E. Identification of transfer function by inverse analysis of self-excited chatter vibration in milling operations. *Precision Engineering-Journal of the International Societies for Precision Engineering and Nanotechnology* **36**, 568-575 (2012). https://doi.org/10.1016/j.precisioneng.2012.04.004

10 Bari, P., Kilic, Z. M., Law, M. & Wahi, P. Rapid stability analysis of serrated end mills using graphical-frequency domain methods. *International Journal of Machine Tools & Manufacture* **171** (2021). https://doi.org/10.1016/j.ijmachtools.2021.103805

11 Farahani, N. D. & Altintas, Y. Chatter Stability of Serrated Milling Tools in Frequency Domain. *Journal of Manufacturing Science and Engineering-Transactions of the Asme* **144** (2022). https://doi.org/10.1115/1.4052007

12 Mohammadi, Y. & Ahmadi, K. Frequency domain analysis of regenerative chatter in machine tools with Linear Time Periodic dynamics. *Mechanical Systems and Signal Processing* **120**, 378-391 (2019). https://doi.org/10.1016/j.ymssp.2018.10.029

13 Safizadeh, M. S., Lakis, A. A. & Thomas, M. in *12th International Congress on Condition Monitoring and Diagnostic Engineering Management.* 125-130 (1999).

14 Peng, Z. K., Tse, P. W. & Chu, F. L. An improved Hilbert-Huang transform and its application in vibration signal analysis. *Journal of Sound and Vibration* **286**, 187-205 (2005). https://doi.org/10.1016/j.jsv.2004.10.005

15 Huang, N. E. *et al.* The empirical mode decomposition and the Hilbert spectrum for nonlinear and non-stationary time series analysis. *Proceedings of the Royal Society a-Mathematical Physical and Engineering Sciences* **454**, 903-995 (1998). https://doi.org/10.1098/rspa.1998.0193

16 Susanto, A. *et al.* Application of Hilbert-Huang transform for vibration signal analysis in end-milling. *Precision Engineering-Journal of the International Societies for Precision Engineering and Nanotechnology* **53**, 263-277 (2018). https://doi.org/10.1016/j.precisioneng.2018.04.008

17 Hochreiter, S. & Schmidhuber, J. Long short-term memory. *Neural Computation* **9**, 1735-1780 (1997). https://doi.org/10.1162/neco.1997.9.8.1735

18 Liu, J. B., Jiang, F., Tashiro, S., Chen, S. J. & Tanaka, M. A physics-informed and data-driven framework for robotic welding in manufacturing. *Nature Communications* **16** (2025). https://doi.org/10.1038/s41467-025-60164-y

19 Sun, Y. X. *et al.* Online chatter detection considering beat effect based on Inception and LSTM neural networks. *Mechanical Systems and Signal Processing* **184** (2023). https://doi.org/10.1016/j.ymssp.2022.109723

20 Gao, H. N. *et al.* Multi-modal denoised data-driven milling chatter detection using an optimized hybrid neural network architecture. *Scientific Reports* **15** (2025). https://doi.org/10.1038/s41598-025-88242-7

21 Vaswani, A. *et al.* in *31st Annual Conference on Neural Information Processing Systems (NIPS).* (2017).

22 Liu, C. F., Wang, D. H., Lin, Y. R. & Song, S. Y. Research on online monitoring of chatter based on continuous wavelet transform and convolutional neural network-vision transformer (CNN-ViT). *Mechanical Sciences* **16**, 167-180 (2025). https://doi.org/10.5194/ms-16-167-2025

23 Zhan, D. N., Lu, D. W., Gao, W. X., Wei, H. J. & Sun, Y. W. Chatter Detection in Thin-Wall Milling Based on Multi-Sensor Fusion and Dual-Stream Residual Attention CNN. *Machines* **12** (2024). https://doi.org/10.3390/machines12080559

24 Jauhari, K., Rahman, A. Z., Al Huda, M., Widodo, A. & Prahasto, T. A hybrid deep learning-based approach for on-line chatter detection in milling using deep stem-inception networks and residual channel-spatial attention mechanisms. *Mechanical Systems and Signal Processing* **226** (2025). https://doi.org/10.1016/j.ymssp.2025.112357

25 Wang, Y. Q. *et al.* Multi-scale enhancement and chatter prediction of milling vibration signals from thin-walled parts based on attentional representation enhancement network. *Mechanical Systems*

and Signal Processing **225** (2025). https://doi.org/10.1016/j.ymssp.2025.112302

26 Vashisht, R. K. & Peng, Q. J. Online Chatter Detection for Milling Operations Using LSTM Neural Networks Assisted by Motor Current Signals of Ball Screw Drives. *Journal of Manufacturing Science and Engineering-Transactions of the Asme* **143** (2021). https://doi.org/10.1115/1.4048001

27 Tobias, S. A. *Machine Tool Vibration*. (John Wiley & Sons Inc, 1973).

28 Li, Z. Q., Wang, Z. K. & Shi, X. F. Fast prediction of chatter stability lobe diagram for milling process using frequency response function or modal parameters. *International Journal of Advanced Manufacturing Technology* **89**, 2603-2612 (2017). https://doi.org/10.1007/s00170-016-9959-4

29 Merdol, S. D. & Altintas, Y. Multi frequency solution of chatter stability for low immersion milling. *Journal of Manufacturing Science and Engineering-Transactions of the Asme* **126**, 459-466 (2004). https://doi.org/10.1115/1.1765139

30 Altintas, Y., Stepan, G., Budak, E., Schmitz, T. & Kilic, Z. M. Chatter Stability of Machining Operations. *Journal of Manufacturing Science and Engineering-Transactions of the Asme* **142** (2020). https://doi.org/10.1115/1.4047391

31 Shivanna, D. M., Kiran, M. B. & Kavitha, S. D. in *International Conference on Advances in Manufacturing and Materials Engineering (ICAMME).* 2132-2141 (2014).

32 Khavieya, A., Bhanuteja, G. V., Chowdhury, S., Arunachalam, N. & Ganesan, A. R. Quantification of Surface Roughness Using Fringe Projection Profilometry for Metallic Machined Surfaces. *J. Tribology (USA)* **147**, 114202-114202 (2025). https://doi.org/10.1115/1.4068171

33 Peters, J. *et al.* Contribution of CIRP to the development of metrology and surface quality evaluation during the last fifty years. *Cirp Annals-Manufacturing Technology* **50**, 471-488 (2001). https://doi.org/10.1016/s0007-8506(07)62996-5

34 Wu, X. F., Liu, Y. H., Zhou, X. L. & Mou, A. L. Automatic Identification of Tool Wear Based on Convolutional Neural Network in Face Milling Process. *Sensors* **19** (2019). https://doi.org/10.3390/s19183817

35 Xiao, G. H., Tu, H. Q., Xu, Y. Z., Shao, J. H. & Xiang, D. M. Surface Roughness Prediction Based on CNN-BiTCN-Attention in End Milling. *International Journal of Advanced Computer Science and Applications* **15**, 815-822 (2024).

36 Zhang, X. X. *et al.* Multi-domain data-driven chatter detection in robotic milling under varied robot poses based on directional attention mechanism. *Mechanical Systems and Signal Processing* **227**

(2025). https://doi.org/10.1016/j.ymssp.2025.112406

37 Zhou, G. *et al.* A new algorithm for chatter quantification and milling instability classification based on surface analysis. *Mechanical Systems and Signal Processing* **204** (2023). https://doi.org/10.1016/j.ymssp.2023.110816

38 Zhu, Z. *et al.* in *Journal of Manufacturing Processes* (2025).

39 Gross, K. *et al.* Determination of the surface topography of ball end micro milled material measures. *Engineering Science and Technology-an International Journal-Jestech* **24**, 543-555 (2021). https://doi.org/10.1016/j.jestch.2020.08.005

40 Zhuo, Y., Han, Z. Y., An, D. & Jin, H. Y. Surface topography prediction in peripheral milling of thin-walled parts considering cutting vibration and material removal effect. *International Journal of Mechanical Sciences* **211** (2021). https://doi.org/10.1016/j.ijmecsci.2021.106797

41 Grossi, N., Scippa, A., Sallese, L., Montevecchi, F. & Campatelli, G. On the generation of chatter marks in peripheral milling: A spectral interpretation. *International Journal of Machine Tools & Manufacture* **133**, 31-46 (2018). https://doi.org/10.1016/j.ijmachtools.2018.05.008